



HAL
open science

Shifting from UV to Visible-Light the Activity of Organic Photoinitiators via the Covalent Grafting of Polyoxometalates

Zeinab El Hajj, Lucie Pierau, Jean-Pierre Malval, Jérôme Marrot, Pierre-Emmanuel Mazeran, Daoud Naoufal, Minh-Huong Ha-Thi, Karine Steenkeste, Anne Dolbecq, Sébastien Floquet, et al.

► To cite this version:

Zeinab El Hajj, Lucie Pierau, Jean-Pierre Malval, Jérôme Marrot, Pierre-Emmanuel Mazeran, et al.. Shifting from UV to Visible-Light the Activity of Organic Photoinitiators via the Covalent Grafting of Polyoxometalates. *Macromolecules*, 2023, 56 (15), pp.6105-6116. 10.1021/acs.macromol.3c00828 . hal-04180587

HAL Id: hal-04180587

<https://hal.science/hal-04180587>

Submitted on 7 Nov 2023

HAL is a multi-disciplinary open access archive for the deposit and dissemination of scientific research documents, whether they are published or not. The documents may come from teaching and research institutions in France or abroad, or from public or private research centers.

L'archive ouverte pluridisciplinaire **HAL**, est destinée au dépôt et à la diffusion de documents scientifiques de niveau recherche, publiés ou non, émanant des établissements d'enseignement et de recherche français ou étrangers, des laboratoires publics ou privés.

Shifting from UV to visible-light the activity of organic photo- initiators via the covalent grafting of polyoxometalates

Zeinab El Hajj,^{a,b} Lucie Pierau,^c Jean-Pierre Malval,^d Jérôme Marrot,^a Pierre-Emmanuel Mazeran,^e
Daoud Naoufal,^b Minh-Huong Ha-Thi,^f Karine Steenkeste,^f Anne Dolbecq,^a Sébastien Floquet,^a Olivier
Oms,^a Davy-Louis Versace^{c,*} and Pierre Mialane^{a,*}

^a Institut Lavoisier de Versailles, UMR 8180, Université Paris Saclay, Université de Versailles Saint-
Quentin en Yvelines, 45 Avenue des Etats-Unis, 78035 Versailles cedex, France.

^b Laboratory of Organometallic and coordination chemistry, LCIO, Lebanese University, Faculty of
Sciences I, Hadath, Lebanon.

^c Univ. Paris-Est Créteil, CNRS, ICMPE, UMR 7182, 2 rue Henri Dunant, 94320 Thiais, France.

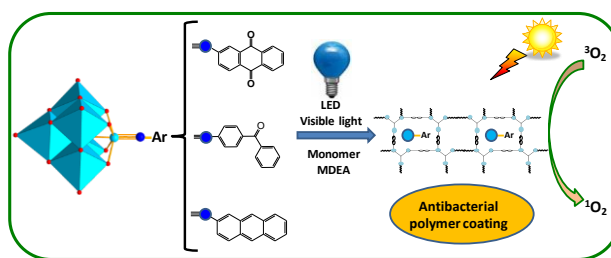
^d Institut de Science des Matériaux de Mulhouse (IS2M), IS2M-LRC 7228, 15 rue Jean Starcky, 68057
Mulhouse, France.

^e Laboratoire Roberval, UMR CRNS-UTC 7337, Centre de Recherche de Royallieu, Université de
Technologie de Compiègne, Compiègne 60205 CEDEX, France.

^f Institut des Sciences Moléculaires d'Orsay (ISMO), UMR 8214, Université Paris-Saclay, Bâtiment 520,
91405 Orsay, France.

*Emails: davy-louis.versace@u-pec.fr, pierre.mialane@uvsq.fr.

TOC (for Table of Contents use only):



Abstract. Anthracene, benzophenone and anthraquinone-based UV photoinitiators have been, respectively, covalently grafted on the $[\text{Mo}_6\text{O}_{19}]^{2-}$ polyoxometalate (POM) platform, affording highly colored charge transfer organo-imido Lindqvist complexes. It has been evidenced that photosystems combining N-methyldiethanolamine (MDEA) as electron donor and these hybrid POMs promote free-radical photopolymerization of acrylate monomer derivatives under irradiation in the visible range, while in similar conditions no polymerization was observed considering as photoinitiators a mixture of the organic and POM precursors. After 800 s, acrylate conversion yields up to 90% under 405 nm LED irradiation and 50% under 470 nm LED irradiation were thus obtained considering the POM-imidoanthraquinone (**POM-AQ**) compound. This evidences that such organo-imido Lindqvist species can represent new easy-to-synthesize, efficient visible-light photoinitiators. Moreover, due to the presence of the POM, coatings prepared using the **POM-AQ**/MDEA/Soybean oil epoxidized acrylate photosystem exhibit excellent mechanical properties, with very good flexibility, resistance to brittle fracture and adherence to the steel. Finally, **POM-AQ** was shown to have a remarkable capacity to generate singlet oxygen species under visible light irradiation, and the antibacterial activity against *S. aureus* under solar light of the related POM-derived surface has been demonstrated.

Introduction. Polyoxometalates (POMs) are soluble anionic metal oxide clusters of d-block transition metals in high oxidation states (typically W^{VI} or Mo^{VI}) exhibiting properties that can be exploited in numerous fields,¹⁻³ these species being, for example, relevant for photochemical⁴ or biological⁵ applications due in particular to their unique redox behaviors. While the classical acid or alkali salts of POMs are generally highly soluble in water, limiting their recyclability and reusability in important applications such as catalysis,⁶ this disadvantage can be overcome by incorporating them into matrices. For instance, the decatungstate polyanion $[W_{10}O_{32}]^{4-}$ and the seminal $[PMo_{12}O_{40}]^{3-}$ and $[SiMo_{12}O_{40}]^{4-}$ Keggin species, highly recognized for their catalytic properties, have been immobilized into polymers using photopolymerization techniques. In that way, $[W_{10}O_{32}]^{4-}$ POMs were associated with silanes (or borane derivatives) and iodonium salts to promote free-radical cationic photopolymerization of epoxides under polychromatic Hg-Xe irradiation.⁷ Similar results were obtained with the three-component photo-initiating systems $[XMo_{12}O_{40}]^{n-}$ ($X = P, n = 3$ or $X = Si, n = 4$) / hydrogen donors (silane, germane) / iodonium salts for initiating the radical and cationic polymerization of acrylates and epoxides under UV irradiation, respectively.⁸ The reduction of iodonium salts by $[PMo_{12}O_{40}]^{3-}$ generates phenyl radicals ($Ph\bullet$) which are involved in a H-abstraction reaction process with silane (or germane) thus forming initiating silyl (or germyl) radicals for free-radical polymerization of acrylate monomers. Subsequently, the oxidation of silyl (or germyl) radicals by iodonium salt leads to initiating cationic reactive species, which can afford the free radical promoted cationic photopolymerization. More recently, new structures of onium salts containing polyoxomolybdates or polyoxotungstates as counter anions were elegantly proposed.⁹ Interestingly, POM derivatives proved to be effective for sensitizing iodonium salts by intramolecular electron transfer reaction under UV irradiation, generating radical and cationic species for synthesizing interpenetrated epoxy/acrylate materials under air conditions. Moreover, the elaborated POM-containing polymers have also proved to be highly active for the degradation of pharmaceutical compounds or the degradation of dyes.¹⁰⁻¹² Noticeably, all the photosystems described above consist in a mixture of anionic POMs with cationic photoinitiators (PIs), allowing photopolymerization under irradiation with $\lambda \leq 405$ nm and leading to

POM-incorporating composites. However, to the best of our knowledge, covalent association of POMs and PIs has never been investigated, although such association could bring new optical properties to the photosystem.

The reaction between the Lindqvist POM $[\text{Mo}_6\text{O}_{19}]^{2-}$ and organic amines, leading to imido derivatives, has been widely studied over the last two decades. As early as 2001, Peng et al. reported a protocol allowing to obtain such hybrid species in high yield.¹³ We can discuss their optical properties, taking as an example the naphthalene derivative $[\text{Mo}_6\text{O}_{18}\text{N}(\text{C}_{10}\text{H}_7)]^{2-}$. The lowest energy electronic transitions are observed at 300 nm for the 2-naphthaleneamine ligand and at 325 nm for the $[\text{Mo}_6\text{O}_{19}]^{2-}$ precursor, respectively. This last transition was assigned to a charge-transfer from the oxygen π -type HOMO to the molybdenum π -type LUMO. Strikingly, in the hybrid complex $[\text{Mo}_6\text{O}_{18}\text{N}(\text{C}_{10}\text{H}_7)]^{2-}$, this band becomes more intense and is bathochromically shifted by nearly 60 nm ($\lambda_{\text{max}} = 383$ nm). This originates from the charge-transfer transition of the coordinated N atom to the molybdenum atom as a result of the delocalization of the π -electrons of the naphthalene ring to the hexamolybdate unit, and evidences a strong electronic interaction between the POM and the covalently bonded organic conjugated ligand.¹⁴ Obviously, the amplitude of the shift strongly depends on the π -electrons delocalization characterizing the organic sub-unit. It follows that such functionalization allows to tune the POM and organic substrate optical properties, and while the yellow $[\text{Mo}_6\text{O}_{19}]^{2-}$ precursor only poorly absorbs in the visible domain, strongly colored hybrid species can be obtained after the grafting of such colorless aromatic amines. However, to the best of our knowledge, the potentiality of such functionalized POMs to act as photoactive species in the visible range has never been explored.

We report herein the synthesis of three new imido derivatives obtained from the $[\text{Mo}_6\text{O}_{19}]^{2-}$ precursor and amino derivatives of the anthracene, benzophenone and anthraquinone photoinitiators, respectively. While these organic PIs are only active under UV irradiation for the polymerization processes targeted in our study, we show that their performances can indeed be strongly increased once connected to the POM unit. Importantly, this represents a novel strategy for shifting the organic

photoinitiator activity from UV to visible light irradiation. The three isolated hybrid materials have been fully characterized both in the solid-state and in solution. Their optical and photophysical properties have been deeply studied by UV-vis spectroscopy, cyclic voltammetry, fluorescence and laser flash photolysis experiments. Their use for the free-radical polymerization of trimethylolpropane triacrylate (TMPTA) and soybean oil epoxidized acrylate (SOA) has been also investigated by Real-Time Fourier Transform InfraRed Spectroscopy (RT-FTIR) and electron paramagnetic resonance spin-trapping (EPR ST). The influence of such POM derivatives on the mechanical properties of the obtained hybrid polymers is discussed. Finally, the antibacterial properties of such materials against *S. aureus* under solar light irradiation are described.

Experimental section.

All chemicals and solvents for synthesis and characterizations were purchased from commercial sources except $(TBA)_2[Mo_6O_{19}]$ (TBA = tetrabutyl ammonium) which has been synthesized as previously described.¹⁵

Synthesis of the molecular compounds.

Synthesis of $(TBA)_2[Mo_6O_{18}(NC_6H_4C(O)C_6H_5)]$ (**POM-AB**). Under an inert atmosphere, $(TBA)_2[Mo_6O_{19}]$ (0.887 g, 0.65 mmol), 2-aminobenzophenone (0.128 g, 0.65 mmol, 1 eq) and N,N'-dicyclohexylcarbodiimide (DCC) (0.188 g, 0.91 mmol, 1.4 eq.) were suspended in 8 mL of anhydrous DMSO. The pale yellow mixture was heated at 70°C for 1 hour, turning dark-red with time. Once the suspension cooled down to room temperature, the mixture was filtered to remove the dicyclohexylcarbodiurea. The resulting filtrate was then added into a flask containing diethyl ether (200 mL), leading to the precipitation of the crude product as an orange powder which was recrystallized from hot acetonitrile (ca. 50°C, 10 mL). Orange crystals of **POM-AB** were then isolated by filtration and washed with ethanol and diethyl ether (0.709 g, 0.46 mmol, yield 71%). ¹H NMR (CD₃CN, 300 MHz): δ

= 7.84-7.19 (m, 9H, anthracene group), 3.12 (t, 16H, TBA), 1.62 (m, 16H, TBA), 1.39 (m, 16H, TBA), 0.98 (t, 24H, TBA). FT-IR (cm⁻¹): 2958 (s), 2933 (s), 2871 (s), 1656 (s), 1598 (m), 1581 (w), 1480 (s), 1377 (m), 1330 (m), 1315 (m), 1292 (m), 1273 (m), 1166 (w), 1151 (w), 1106 (w), 1025 (w), 976 (m, v(Mo-N)), 944 (s, v(Mo-O_i)), 924 (sh), 879 (w), 764 (s, v(Mo-O_b-Mo)), 588 (s). ESI/MS: [Mo₆O₁₉]²⁻ m/z = 439.67 (exp.), m/z = 440.15 (calc.); [Mo₆O₁₈(NC₆H₄-C(O)-C₆H₅)]²⁻ m/z = 529.20 (exp.), m/z = 529.43 (calc.); ((TBA)[Mo₆O₁₈(NC₆H₄-C(O)-C₆H₅)]⁻ m/z = 1302.70 (exp.), m/z = 1301.31 (calc.). Anal. Calcd for Mo₆O₁₉N₃C₄₅H₈₁ (found) %: C, 35.01 (35.16); H, 5.29 (5.17); N, 2.72 (2.75).

Synthesis of (TBA)₂[Mo₆O₁₈(NC₁₄H₉)] (**POM-AC**). **POM-AC** was synthesized following the same protocol than that described for **POM-AB** but using 2-aminoanthracene (0.125 g, 0.65 mmol, 1 eq) instead of 2-aminobenzophenone. The reddish crude product was recrystallized from hot acetonitrile (ca. 50°C, 3 mL) and isolated by filtration as a red powder which was washed with diethyl ether (0.349 g, 0.23 mmol, yield 35%). Crystals suitable for X-rays diffraction were obtained through diffusion of *tert*-butylmethyl ether into an acetonitrile solution. ¹H NMR (CD₃CN, 300 MHz): δ = 8.51 (d, 2H), 8.07 (m, 3H), 7.87 (s, 1H), 7.55 (m, 2H), 7.40 (dd, 1H), 3.12 (t, 16H, TBA), 1.61 (m, 16H, TBA), 1.36 (m, 16H, TBA), 0.98 (t, 24H, TBA). FT-IR (cm⁻¹): 2960 (s), 2932 (s), 2873 (s), 1480 (s), 1454 (s), 1377 (m), 1343 (m), 1309 (m), 1296 (m), 1239 (w), 1147 (w), 1107 (w), 1068 (w), 1029 (w), 975 (m, v(Mo-N)), 945 (vs, v(Mo-O_i)), 894 (s), 765 (s, v(Mo-O_b-Mo)), 583 (s). ESI/MS: [Mo₆O₁₉]²⁻ m/z = 439.88 (exp.), m/z = 440.15 (calc.); [Mo₆O₁₈(NC₁₄H₉)]²⁻ m/z = 528.19 (exp.), m/z = 527.5 (calc.); ((TBA)[Mo₆O₁₈(NC₁₄H₉)]⁻ m/z = 1296.67 (exp.), m/z = 1297.0 (calc.). Anal. Calcd for Mo₆O₁₈N₃C₄₆H₈₁ (found) %: C, 35.90 (35.72); H, 5.30 (5.20); N, 2.70 (2.74).

Synthesis of (TBA)₂[Mo₆O₁₈(NC₁₄H₇O₂)] (**POM-AQ**). **POM-AQ** was synthesized following the same protocol than that described for **POM-AB** but using 2-aminoanthraquinone (0.145 g, 0.65 mmol, 1 eq) instead of 2-aminobenzophenone. After filtration of the dicyclohexylcarbodiurea, the resulting filtrate was then added into a flask containing diethyl ether (200 mL) and ethanol (50 mL), leading to the precipitation of the crude product as a brown-reddish powder. The powder was collected, washed with

ethanol and dried with ether ($m = 0.856$ g). It was then solubilized in a minimum of acetonitrile. After a few hours, the resulting mixture was filtrated, the solid mainly consisting in unreacted POM precursor. The filtrate was evaporated and **POM-AQ** was isolated as a brown powder after trituration with diethylether (0.450 g). $^1\text{H NMR}$ (CD_3CN , 300 MHz): $\delta = 8.22$ (m, 2.4H), 7.85 (m, 2.4H), 7.53 (dd, 0.8H), 3.16 (t, 16H, TBA), 1.65 (m, 16H, TBA), 1.40 (m, 16H, TBA), 0.98 (t, 24H, TBA). FT-IR (cm^{-1}): 2961 (s), 2933 (s), 2873 (s), 1672 (s), 1574 (s), 1464 (s), 1415 (w), 1379 (m), 1335 (s), 1315 (s), 1284 (s), 1151 (m), 1098 (w), 1063 (w), 977 (m, $\nu(\text{Mo-N})$), 945 (vs, $\nu(\text{Mo-O}_t)$), 852 (w), 765 (s, $\nu(\text{Mo-O}_b\text{-Mo})$), 586 (s). ESI/MS: $[\text{Mo}_6\text{O}_{18}(\text{NC}_{14}\text{H}_7\text{O}_2)]^{2-}$ $m/z = 540.17$ (exp.), $m/z = 542.48$ (calc.); $[\text{H}[\text{O}_{18}\text{Mo}_6(\text{NC}_{14}\text{H}_7\text{O}_2)]]^-$ $m/z = 1085.39$ (exp.), $m/z = 1085.96$ (calc.); $[(\text{TBA})[\text{Mo}_6\text{O}_{18}(\text{NC}_{14}\text{H}_7\text{O}_2)]]^-$ $m/z = 1328.67$ (exp.), $m/z = 1327.42$ (calc.).

Photopolymerization kinetic studies. 2 wt% (with respect to the monomer) of POM derivatives (**POM-AC**, **POM-AB** or **POM-AQ**) were dissolved with 5 wt% (with respect to the monomer) of the reductive co-initiator MDEA in acrylate monomer (TMPTA or SOA). After stirring and sonicating the respective formulations for 5 min, photopolymerizations were performed at room temperature. 12 μm -layers of solution were put down to a BaF_2 pellet and irradiated with LED@385 nm ($44 \text{ mW}\cdot\text{cm}^{-2}$), LED@405 nm ($25 \text{ mW}\cdot\text{cm}^{-2}$), LED@455 nm ($15 \text{ mW}\cdot\text{cm}^{-2}$) or LED @470 nm ($25 \text{ mW}\cdot\text{cm}^{-2}$), under air or in laminate conditions. The Infrared spectra of the sample were continuously recorded by Real-Time Fourier Transform InfraRed Spectroscopy (RT-FTIR) with a JASCO FTIR 4700 Instrument as previously described.¹⁶ The photo-reactivity of the acrylate monomers was observed by following the acrylate functions absorption bands at 1636 cm^{-1} .

Antibacterial Assays. Antibacterial assays were performed with *S. aureus* ATCC6538 on the **POM-AQ** derived materials under solar-light irradiation according to a previously described procedure.¹⁷ The photoinduced materials which have been made with a common UV photoinitiator i.e. 2,2-Dimethoxy-2-phenylacetophenone (DMPA) under UV-light irradiation are used as reference samples for antibacterial tests.

¹H NMR spectra were recorded at 298 K on a Bruker Advance 300 spectrometer operating at 300 MHz. Chemical shifts are expressed in parts per million (ppm) downfield from internal TMS. The following abbreviations were used to explain the multiplicities: s, singlet; d, doublet; t, triplet; br, broad peaks; m, multiplet or overlapping peaks.

Electrospray ionization (ESI) mass spectra were recorded on a Xevo QT of WATERS (quadrupole-time-of-flight) instrument. The temperature of the source block was set to 120 °C, and the desolvation temperature to 200 °C. A capillary voltage of 1 kV was used in the negative scan mode, and the cone voltage was set to 10 V to control the extent of fragmentation of the identified species. Mass calibration was performed using a solution of sodium formate in water:acetonitrile (2:8) from $m/z = 50$ to 3000. Sample solutions 50 $\mu\text{mol/L}$ in acetonitrile were injected via syringe pump directly connected to the ESI source at a flow rate of 20 $\mu\text{L/min}$.

Infrared (IR) spectra were recorded on a Nicolet 30 ATR 6700 FT spectrometer. UV-vis spectra were recorded on a Perkin Elmer Lambda 750 UV/Vis/NIR spectrometer.

X-ray Diffraction. Intensity data collections were carried out with a Bruker D8 VENTURE diffractometer equipped with a PHOTON 100 CMOS bidimensional detector using a high brilliance $1\mu\text{S}$ microfocus X-ray Mo $K\alpha$ monochromatized radiation ($\lambda = 0.71073 \text{ \AA}$). The absorption corrections were based on multiple and symmetry-equivalent reflections in the data sets using the SADABS program¹⁸ based on the method of Blessing.¹⁹ The structures were solved by direct methods and refined by full-matrix least-squares using the SHELX-TL package.²⁰ The hydrogen atoms were theoretically located on the basis of the conformation of the supporting atoms. The crystallographic data are gathered in Table S1. CCDC numbers of **POM-AB** and **POM-AC** are 2257497 and 2257498, respectively. These data can be obtained free of charge from The Cambridge Crystallographic Data Centre via www.ccdc.cam.ac.uk/data_request/cif.

UV-Visible absorption spectra were recorded using a Perkin Elmer Lambda 2 UV-Vis spectrophotometer.

Steady-state photolysis experiments. Fluorescence spectra were recorded from a FluoroMax-4 spectrofluorometer according to previously described method.²¹ The acetonitrile solutions of **POM-AQ**, **POM-AC** and **POM-AB** were irradiated under LED@405 nm (25 mW/cm²) under air, with and without the presence of a reductive co-initiator MDEA to observe their photostability.

Electron Paramagnetic Resonance Spin-trapping (EPR ST) experiments. The X-band cw-EPR spectra (modulation frequency of 100 kHz) were monitored with the EMX*plus* spectrometer (Bruker) equipped with the High Sensitivity Probe-head (Bruker) in the small quartz flat cell (Wilmad-LabGlass, WG 808-Q). The spin trapping agent 5,5-dimethyl-1-pyrroline *N*-oxide (DMPO; Sigma-Aldrich) was distilled prior to the application and dissolved in acetonitrile (ACN; SeccoSolv[®] Merck). The solutions prepared by mixing stock solutions of POM-derivatives, MDEA and DMPO in ACN were carefully saturated by argon and immediately irradiated at 295 K directly in the EPR resonator utilizing a LED@400 nm source ($\lambda_{\text{max}} = 400$ nm; Bluepoint LED, Höppler UV Technology). The EPR spectra were recorded *in situ* during/after a defined exposure. The *g*-factors were determined with an uncertainty of ± 0.0001 exploiting a nuclear magnetic resonance teslameter (ER 036TM, Bruker) and integrated frequency counter. The experimental EPR spectra were analyzed by the WinEPR software (Bruker) and the calculations of spin-Hamiltonian parameters were performed with the EasySpin toolbox working on MatLab[®] platform.²² The standard EPR spectrometer settings were as follows: microwave frequency, ~ 9.427 GHz; microwave power, ~ 11.10 mW or ~ 20.93 mW; center field, ~ 335.8 mT; sweep width, 8–10 mT; gain, 2.00×10^5 ; modulation amplitude, 0.1 mT or 0.05 mT; sweep time, 45 s; time constant, 10.24 ms; the number of scans, 5 or 10.

Cyclic voltammetry. Cyclic voltammetry scans were done according to a previous described procedure.²² Measurements were carried out on acetonitrile solutions of POM derivatives ($C = 10^{-3}$ M) between 0 and 2.15 V for oxidation, and between 0 and -1V for reduction, with a $0.05 \text{ V} \cdot \text{s}^{-1}$ scan rate. The data were analyzed on GPES electrochemical software 4.9 (Utrecht, Netherlands).

Laser Flash Photolysis experiments. Nanosecond transient absorption measurements were performed using a home-built setup which has been described previously.²³ Briefly, a Nd:YAG pumped optical parametric oscillator (OPO) laser was used for sample excitation at 380 nm with an energy of ~ 2 mJ/pulse with a repetition rate of 10 Hz. A white light continuum laser (STM-2-UV LEUKOS) at a repetition rate of 20 Hz was used as a probe. The probe beam was split into two arms, one for probing samples and the other for reference in order to compensate for energy fluctuations. The probing arms were then coupled into a round-to-linear optical fiber bundle before being analyzed by a spectrograph SPEX 270M (Jobin-Yvon). Detection of the dispersed white light was performed by an intensified charge coupled device (ICCD) detector PIMAX 4 (Princeton Instrument). Transient absorption spectra were calculated using the following formula:

$$\Delta A = \log_{10} \left(\frac{S_{ref}^{on}}{S_{ref}^{off}} \times \frac{S_{prob}^{off}}{S_{prob}^{on}} \right)$$

where S_{ref}^{on} and S_{ref}^{off} are reference spectra when pump laser is on and off respectively, S_{prob}^{on} and S_{prob}^{off} are probe spectra when pump laser is on and off respectively.

Nanoindentation experiments. Nanoindentation and scratch experiments were performed on steel substrate coatings at room temperature. A commercial Nano Indenter (G200 from Agilent Technologies) using a Berkovich tip (Micro Star Technologies) were used. Thirty tests were done. Samples were loaded and unloaded at constant strain rate (0.05 s^{-1}) using a home-made method.²⁴ Loading was realized using the Continuous Stiffness Method (CSM) until a $1 \mu\text{m}$ depth was obtained. Unloading was performed after a hold load plateau of 60 s to achieve the viscous response. Twenty parallel scratches face forward distant from $200 \mu\text{m}$ were performed, with a load increasing from 0 to 100 mN on a $500 \mu\text{m}$ length.

DSC measurements. DSC measurements were performed on a TA Instruments DSC25 discovery series with a refrigerated cooling system RCS90.

Dynamic Mechanical Analyses (DMA). DMA experiments were done with a TA Q800 DMA apparatus equipped with a tensile setup to characterize the thermo-mechanical behavior of the POM derived samples according to a previous procedure.²⁵ Experiments were performed in a closed environment and samples were cooled down to -140 °C and heated up to 50 °C with a 3 °C/min ramp rate. The applied stress frequency was 1 Hz, with a 0.1% deformation and a pre-load static force of 0.01 N.

Singlet oxygen species detection. The singlet oxygen photogeneration by **POM-AQ** was investigated in solution using tetraphenylcyclopentadienone (TPCPD). The progress of reactive oxygen species (ROS) generation was followed by the oxidation of TPCPD, hence by the subsequent decrease of its absorbance at 495 nm. A solution containing both TPCPD (6.29×10^{-4} M) and **POM-AQ** (4.97×10^{-5} M) was prepared in ACN. The solution was irradiated with a LED@405 nm (25 mW/cm^2) and sampled at fixed times to monitor the decrease of the TPCPD absorption by UV-visible spectroscopy. The reference test consists in the irradiation of TPCPD alone in ACN without **POM-AQ**, to observe its own photobleaching during the irradiation.

Results and Discussion.

Synthesis and characterization of the hybrid POMs. The synthesis of monosubstituted organoimido POM derivatives has been well-developed during the last two decades. Our strategy follows the main synthetic route which proceeds via a N,N'-dicyclohexylcarbodiimide (DCC)-mediated POM-amine coupling reaction.¹³ First, many attempts were performed by reacting the octamolybdate polyanion $[\text{Mo}_8\text{O}_{26}]^{4-}$ with aromatic amines (2-aminoanthracene, 2-aminoanthraquinone or 2-aminobenzophenone) or their ammonium forms in presence of DCC in refluxing acetonitrile. Unfortunately, hard-to-define mixtures were systematically obtained, prompting us to modify the experimental conditions (nature of the POM precursor, temperature...), in particular using DMSO instead of acetonitrile as solvent as recently successfully considered by Fielden and coll. for the synthesis of several related hybrids.²⁶⁻²⁹

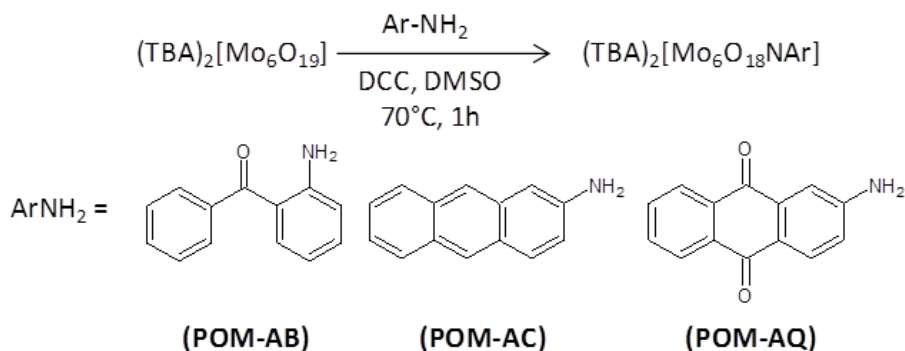


Figure 1. Synthetic pathway of the organoimido POM derivatives **POM-AB**, **POM-AC** and **POM-AQ**.

Thus, by reacting in hot anhydrous DMSO (70°C) and in presence of DCC the Lindqvist-type polyanion $(TBA)_2[Mo_6O_{19}]$ (TBA = tetrabutylammonium) with the corresponding amines (Figure 1), $(TBA)_2[Mo_6O_{18}(NC_6H_4C(O)C_6H_5)]$ (**POM-AB**), $(TBA)_2[Mo_6O_{18}(NC_{14}H_9)]$ (**POM-AC**) and $(TBA)_2[Mo_6O_{18}(NC_{14}H_7O_2)]$ (**POM-AQ**) could be isolated as highly colored solids. Notably, these complexes were optimally obtained in a very short reaction time (1 h) in contrast to previously reported POM imido derivatives, whose synthesis usually required at least 10 h. ^1H NMR spectroscopy appears as an appropriate tool to evidence the efficiency of the coupling reaction. First, the ^1H NMR spectra of each compound unambiguously show that the covalent grafting of the organic part onto the POM platform induces a strong variation of the chemical shifts of the protons in the aromatic range (Figures S1-S6). This general downfield shift underlines the electron withdrawing effect of the inorganic matrix. Obviously, these spectra can easily evidence the potential presence of unreacted amine in the final product. In addition, the coupling efficiency can be evaluated by measuring the ratio between the integration of the signals of the aromatic organic part (in the 5-9 ppm range) and of those related to the TBA cations (in the 0.9-3.5 ppm range), each of these three hybrid POMs containing two tetrabutylammonium counter-cations for one organic fragment. The organic group / TBA ratio of 0.5 determined for both **POM-AB** and **POM-AC** perfectly matches the expected value. In contrast, a ratio of 0.4 is observed for **POM-AQ**, indicating the presence of ca. 20% of unreacted $(TBA)_2[Mo_6O_{19}]$ in the

isolated material. Despite numerous efforts, it has not been possible to fully remove this precursor impurity. The infrared spectra of **POM-AB**, **POM-AC**, **POM-AQ** and the POM precursor in the 500-1800 cm^{-1} range (Figure S7) can be divided into two regions. In the first region above 1000 cm^{-1} , numerous new stretching bands appear in the spectra of the hybrid POMs compared to that of $(\text{TBA})_2[\text{Mo}_6\text{O}_{19}]$ which only contains bands belonging to the TBA cations. These new bands evidence the presence of the organic moieties in the final products. In the second region below 1000 cm^{-1} the bands mainly characterize the inorganic platform. The $\nu(\text{Mo}-\text{O}_t)$ and $\nu(\text{Mo}-\text{O}_b-\text{Mo})$ are located at 951 cm^{-1} and 783 cm^{-1} respectively for $(\text{TBA})_2[\text{Mo}_6\text{O}_{19}]$. These stretching vibrations are bathochromically shifted to 945 ± 1 cm^{-1} and 765 ± 1 cm^{-1} for the title complexes. Such typical variations indicate that Mo-O bonds are weaker in the hybrid POMs due to the formation of a strong new Mo-N bond. Importantly, a new vibration band at 976 ± 1 cm^{-1} , not present in the spectrum of $(\text{TBA})_2[\text{Mo}_6\text{O}_{19}]$, is observed for these hybrids. It is attributed to the Mo-N stretching vibration, thus confirming the formation of organoimido POM derivatives. The ESI/MS spectra of the three functionalized polyoxometalates solubilized in acetonitrile also support the successful synthesis of the targeted products. Indeed, for **POM-AB**, the isotopic peaks centered at $m/z = 529.20$ can be assigned to the anion $[\text{Mo}_6\text{O}_{18}(\text{NC}_6\text{H}_4-\text{C}(\text{O})-\text{C}_6\text{H}_5)]^{2-}$ while the peak at $m/z = 1301.70$ corresponds to the anionic aggregate $((\text{TBA})[\text{Mo}_6\text{O}_{18}(\text{NC}_6\text{H}_4-\text{C}(\text{O})-\text{C}_6\text{H}_5)])^-$ (Figure S8). Analogously, for **POM-AC**, the peak related to the inorganic part $[\text{Mo}_6\text{O}_{18}(\text{NC}_{14}\text{H}_9)]^{2-}$ is observed at $m/z = 528.19$ and the isotopic peaks centered at $m/z=1296.67$ can be attributed to the $((\text{TBA})[\text{Mo}_6\text{O}_{18}(\text{NC}_{14}\text{H}_9)])^-$ aggregate resulting from the association of the dianion and a TBA cation (Figure 2a). Lastly, for **POM-AQ**, the isotopic peaks at $m/z = 540.17$ and $m/z = 1328.68$ correspond to $[\text{Mo}_6\text{O}_{18}(\text{NC}_{14}\text{H}_7\text{O}_2)]^{2-}$ and $((\text{TBA})[\text{Mo}_6\text{O}_{18}(\text{NC}_{14}\text{H}_7\text{O}_2)])^-$ respectively while the peak at $m/z = 1086.39$ can be assigned to $(\text{H}[\text{Mo}_6\text{O}_{18}(\text{NC}_{14}\text{H}_7\text{O}_2)])^-$ (Figure S9). Importantly, these data indicate that the three reported species are stable in acetonitrile solution.

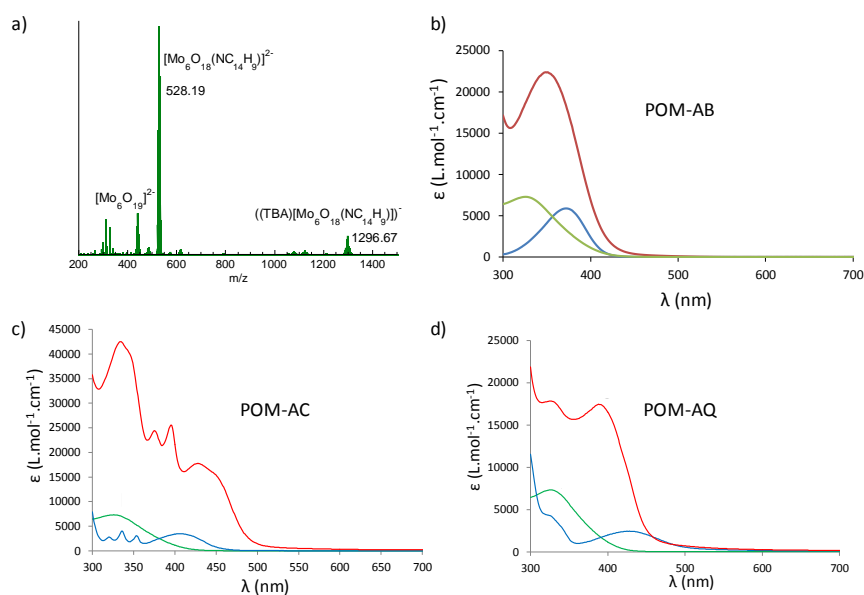


Figure 2. a) ESI-MS spectrum of **POM-AC** in acetonitrile, and UV-Visible spectra in acetonitrile of b) 2-aminobenzophenone (blue line), $(\text{TBA})_2[\text{Mo}_6\text{O}_{19}]$ (green line) and **POM-AB** (red line); c) 2-aminoanthracene (blue line), $(\text{TBA})_2[\text{Mo}_6\text{O}_{19}]$ (green line) and **POM-AC** (red line) and d), 2-aminoanthraquinone (blue line), $(\text{TBA})_2[\text{Mo}_6\text{O}_{19}]$ (green line) and **POM-AQ** (red line).

The UV-Vis absorption spectra of the three hybrid compounds and the related organic and inorganic precursors were recorded in acetonitrile. First of all, the lowest energy absorption band of the Lindqvist-type polyanion $(\text{TBA})_2[\text{Mo}_6\text{O}_{19}]$ located at $\lambda = 325$ nm is attributed to the Ligand-to-Metal charge transfer (LMCT) from the oxygen π -type highest occupied molecular orbital (HOMO) to the molybdenum π -type lowest unoccupied molecular orbital (LUMO). In **POM-AB**, this band is bathochromically shifted of 24 nm ($\lambda = 349$ nm) and above all, considerably more intense (Figure 2b). Considering as an example the ϵ values for $\lambda = 405$ nm (one of the wavelength values tested for photopolymerization processes, see below), we actually observe a significant difference between **POM-AB** ($\epsilon_{405} = 5300$ L.mol⁻¹.cm⁻¹) and 2-aminobenzophenone ($\epsilon_{405} = 1660$ L.mol⁻¹.cm⁻¹). This is in accordance with optical properties of previously reported arylimido POM derivatives and results from the enhanced delocalization of the aromatic π -electrons to the inorganic matrix *via* the formation of

the Mo≡N triple bond.¹⁴ In the UV-Vis spectrum of 2-aminoanthracene, the lowest absorption band is located at 406 nm while **POM-AC** exhibits a broad and intense absorption band at 428 nm along with a shoulder at 449 nm (Figure 2c), indicating that these species absorb in the visible domain. Globally, all of the electronic transition bands of the precursors are red-shifted demonstrating here again the strong electronic interaction between the two components. Notably, the increase of the ϵ values is strongly pronounced for **POM-AC**, with $\epsilon_{405} = 17230 \text{ L}\cdot\text{mol}^{-1}\cdot\text{cm}^{-1}$ against $\epsilon_{405} = 3480 \text{ L}\cdot\text{mol}^{-1}\cdot\text{cm}^{-1}$ for 2-aminoanthracene. This is also the case for **POM-AQ** with ϵ_{405} value up to ca. $15600 \text{ L}\cdot\text{mol}^{-1}\cdot\text{cm}^{-1}$, much higher than that of the organic precursor ($\epsilon_{405} = 2100 \text{ L}\cdot\text{mol}^{-1}\cdot\text{cm}^{-1}$) (Figure 2d).

Single crystal X-ray diffraction studies confirm that in **POM-AC** and **POM-AB** the organic moiety is covalently linked to the hexamolybdate core through the nitrogen atom. For **POM-AB**, the short formed Mo-N bonds ($1.7392(1) \text{ \AA}$) along with the C-N-Mo angle ($170.361(4)^\circ$) are illustrative of organoimido groups bound to an octahedral d^0 metal center *via* a Mo≡N triple bond (Figure 3, bottom). This is also the case for **POM-AC** but the Mo-N bond is slightly longer ($1.7737(1) \text{ \AA}$) while the more acute C-N-Mo angle ($154.597(4)^\circ$) evidences a stronger distortion, probably due to the steric hindrance of the anthracene group (Figure 3, top). Also, as a typical feature for organoimido POM derivatives, the bond between the central oxygen and the molybdenum bearing the organic moiety is significantly shorter ($2.2167(1) \text{ \AA}$ for **POM-AB** and $2.2058(1) \text{ \AA}$ for **POM-AC**) than the bonds between the central oxygen and the five other metal centers (in the $2.3183(1)$ - $2.3625(1) \text{ \AA}$ range for **POM-AB** and in the $2.3078(1)$ - $2.3775(1) \text{ \AA}$ range for **POM-AC**). The crystal packing of **POM-AC** does not exhibit any π - π interactions between neighboring anthracene units nor between the aromatic group and the nearest POM facet. In contrast, as it can be seen in Figure S10, π - π interactions involving the monosubstituted aromatic ring of two adjacent benzophenone moieties leads to the formation of dimers along the z axis in **POM-AB**. These interactions are characterized by a distance of $3.8063(1) \text{ \AA}$ between the centroids of these parallel rings.

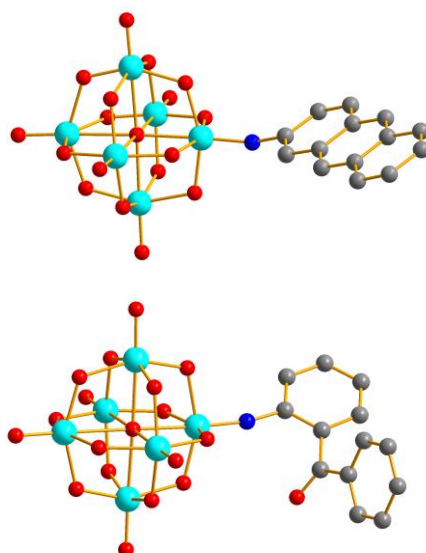


Figure 3. Molecular structures of **POM-AC** (top) and **POM-AB** (bottom). TBA cations and H atoms have been omitted for clarity. Turquoise spheres: Mo, red spheres: O, blue spheres: N, grey spheres: C.

Once these new hybrid POMs fully characterized, the photophysical properties of photosystems made of the **POM-AC**, **POM-AB** and **POM-AQ** complexes, respectively, and *N*-methyldiethanolamine (MDEA) as reducing agent have been studied, and the relevance of these hybrids as PIs for acrylate monomer photopolymerization under visible-light LED irradiation has also been investigated.

Photochemical characterization of the new photoinitiating systems based on POM derivatives.

Steady-state photolysis. First, steady-state photolysis has been used to observe the electronic interaction of the reported complexes with the reductive agent selected for the free-radical polymerization experiments, *e.g.* MDEA. The photolysis of **POM-AB**, **POM-AC** and **POM-AQ** alone and in the presence of MDEA under LED@405nm is reported in Figures 4 and S11. In absence of MDEA, the only very slight absorbance decrease under LED irradiation of the LMCT bands located at ca. 400 nm and characterizing the POM derivatives highlights their high photostability (Figures 4a, S11a and S11c). In contrast, in presence of MDEA, a dramatic decrease of the absorbance of these bands is observed

(Figures 4b, S11b and S11d), suggesting a photoinduced electron transfer reaction between the three POMs, respectively, and MDEA, as described in the following section.

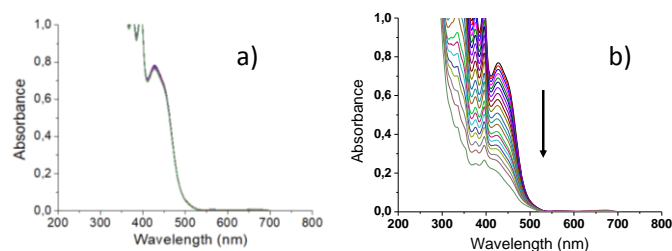


Figure 4. Photolysis of a) **POM-AC** alone and b) **POM-AC/MDEA** in acetonitrile under LED@405nm in the 0-600 s range. Light intensity = 25 mW.cm⁻². [MDEA] = 55 mM and [POM-AC] = 5.3 10⁻⁵ M.

Reactivity of POM derivatives at the excited states. In order to evaluate the reactivity of POM derivatives at their singlet excited state, fluorescence experiments have been performed. Regarding the possibility of electron transfer reactions between POM derivatives and MDEA, cyclic voltammetry experiments in acetonitrile have also been done (Figure S12). All the determined photophysical data are summarized in Table 1.

Regarding **POM-AQ**, a maximum of fluorescence is observed at 604 nm ($\lambda_{\text{ex}} = 420$ nm), with a fluorescence quantum yield of $\Phi_{\text{fluo}} = 0.013$. The gradual addition of MDEA to **POM-AQ** leads to a decrease of fluorescence (Figure 5) with a quite high Stern-Volmer constant $K_{\text{SV}}^{\text{MDEA}} = 8.7 \text{ M}^{-1}$. Associated electron transfer yield ϕ_{eT} calculated from the equation $\phi_{\text{eT}} = K_{\text{SV}}^{\text{MDEA}} \times [\text{MDEA}] / (1 + K_{\text{SV}}^{\text{MDEA}} \times [\text{MDEA}])$ afforded $\phi_{\text{eT}} = 0.812$ for [MDEA] = 0.495 M, *e.g.* for the MDEA concentration used in the kinetics of photopolymerization conditions (see below). This calculated ϕ_{eT} value is relatively high, demonstrating thus a favorable electron transfer reaction between the singlet excited state of **POM-AQ** and MDEA. This result is not surprising as Rehm-Weller equation (see equation S1) which is used to determine if the electron transfer reaction from MDEA to **POM-AQ** is possible in the excited singlet state predicted favorable **POM-AQ/MDEA** interaction using the oxidation potential of MDEA

($E_{\text{ox}}(\text{MDEA}) = +1.00 \text{ V/SCE}$), the reduction potential of **POM-AQ** ($E_{\text{red}}(\text{POM-AQ}) = -0.38 \text{ V/SCE}$) and its excited singlet-state energy ($E_s(\text{POM-AQ}) = 2.48 \text{ eV}$, corresponding to the maximum of the fluorescence emission spectrum (Figure 5)), the $\Delta G_S(\text{POM-AQ/MDEA})$ free energy change value for the electron transfer reaction being indeed estimated to -1.10 eV (Table 1).

Regarding **POM-AQ**, a maximum of fluorescence is observed at 604 nm ($\lambda_{\text{ex}} = 420 \text{ nm}$), with a fluorescence quantum yield of $\Phi_{\text{fluo}} = 0.013$. The gradual addition of MDEA to **POM-AQ** leads to a decrease of fluorescence (Figure 5) with a quite high fluorescence constant $K_{\text{SV}}^{\text{MDEA}} = 8.7 \text{ M}^{-1}$. Associated electron transfer yield ϕ_{eT} calculated from the equation $\phi_{\text{eT}} = K_{\text{SV}}^{\text{MDEA}} \times [\text{MDEA}] / (1 + K_{\text{SV}}^{\text{MDEA}} \times [\text{MDEA}])$ afforded $\phi_{\text{eT}} = 0.812$ for $[\text{MDEA}] = 0.495 \text{ M}$, *e.g.* for the MDEA concentration used in the kinetics of photopolymerization conditions (see below). This calculated ϕ_{eT} value is relatively high, demonstrating thus a favorable electron transfer reaction between the singlet excited state of **POM-AQ** and MDEA. This result is not surprising as Rehm-Weller-equation (see equation S1) which is used to determine if the electron transfer reaction from MDEA to **POM-AQ** is possible in the excited singlet state predicted favorable **POM-AQ/MDEA** interaction using the oxidation potential of MDEA ($E_{\text{ox}}(\text{MDEA}) = +1.00 \text{ V/SCE}$), the reduction potential of **POM-AQ** ($E_{\text{red}}(\text{POM-AQ}) = -0.38 \text{ V/SCE}$) and its excited singlet-state energy ($E_s(\text{POM-AQ}) = 2.48 \text{ eV}$, corresponding to the maximum of the fluorescence emission spectrum (Figure 5)), the $\Delta G_S(\text{POM-AQ/MDEA})$ free energy change value for the electron transfer reaction being indeed estimated to -1.10 eV (Table 1). Surprisingly, no fluorescence was observed neither for **POM-AB** nor **POM-AC**, avoiding the estimation of the fluorescence quenching by MDEA. Thus, the excited singlet-state energies of **POM-AB** and **POM-AC** have been estimated from the UV absorption band edge, being evaluated to 2.58 eV and 2.36 eV , respectively. Interestingly, $\Delta G_S(\text{POM-AC/MDEA})$ and $\Delta G_S(\text{POM-AB/MDEA})$ are negative, demonstrating also a favorable electron transfer reaction between both POM derivatives and MDEA.

Table 1. Photophysical properties of **POM-AC**, **POM-AB** and **POM-AQ**.

λ_{maxfluo} (nm)	Φ_{fluo}	E_s (eV)	$K_{\text{SV}}^{\text{MDEA}}(\text{M}^{-1})$	E_{ox} (V)	E_{red} (V)	$\Delta G_S(\text{POM/MDEA})$ (eV)
------------------------------------	----------------------	------------	--	---------------------	----------------------	------------------------------------

POM-AC	-	-	2.36*	-	1.14; 1.32	-0.57	-0.79 < 0
POM-AB	-	-	2.58*	-	1.79; 1.91	-0.58	-1 < 0
POM-AQ	604	0.013	2.48	8.7	1.40	-0.38	-1.1 < 0
MDEA	-	-	-	-	1	-	-

*estimated from the UV absorption band edge, Φ_{fluor} = fluorescence quantum yield, E_S = excited singlet state energy, $K_{\text{SV}}^{\text{MDEA}}$ = quenching of fluorescence by MDEA, E_{ox} = oxidation potential of the electron donor, E_{red} = the reduction potential of the electron acceptor and ΔG_s (POM/MDEA) = free energy change value for the electron transfer reaction. E_{ox} and E_{red} values are referred to the SCE electrode.

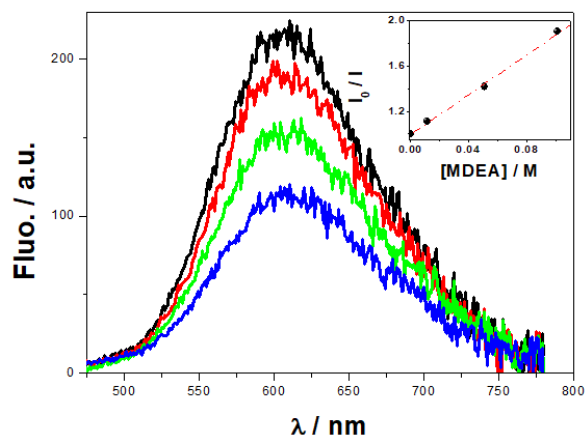


Figure 5. Quenching of **POM-AQ** fluorescence upon gradual addition of MDEA (from black to blue curve) in acetonitrile ($\lambda_{\text{ex}} = 420$ nm). Inset: corresponding Stern-Volmer plot. Absorbance of **POM-AQ** at 425 nm = 0.05.

Transient absorption spectra obtained under excitation at 380 nm evidenced the presence of a large absorption band between 400 nm and 800 nm starting from 100 ns to 40 ms delay times for the three reported hybrid POMs (Figures 6, S13 and S14 for **POM-AQ**, **POM-AB** and **POM-AC**, respectively).

Focusing first on the **POM-AQ** compound, we observe an absorption band at about 450 nm in the early time (Figure 6, left). This band decays rapidly, in several nanoseconds, and can be attributed to the singlet state absorption of the anthraquinone moiety. Then, a large absorption band between 400 nm and 800 nm appears in less than 100 ns until 40 ms delay times. It is generally assumed that when anthraquinone is functionalized with electron-donor groups (amine functional group), the lowest excited states show a strong charge transfer (CT) character.³⁰ This band mainly results from the conjugation of the free electron pair located on the p_z orbital of the nitrogen with the π electronic system of anthraquinone. In the presence of the POM moiety, the lifetime associated with this CT band

is evaluated to be 15 ± 4 ms for **POM-AQ** (Figure 6, right). This long-lived CT state could be an intermediate in photoinduced electron transfer reactions between POM-derivatives and MDEA. Similar results of long-lived CT in the millisecond time scale were obtained for **POM-AB** (CT lifetime = 21 ± 6 ms) and **POM-AC** (CT lifetime = 17 ± 5 ms). However, no singlet state at short delay times was observed in the case of **POM-AB** and **POM-AC**, which is in agreement with the absence of the fluorescence in these compounds (Figures S13 and S14).

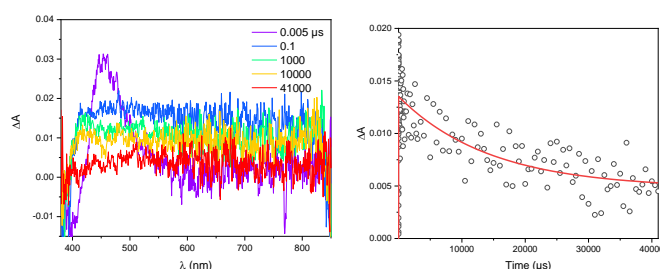


Figure 6. Transient absorption spectra at indicated delay times (left) and the kinetic trace at 500 nm (right) of **POM-AQ** in acetonitrile ($[\text{POM-AQ}] = 2.7 \times 10^{-5}$ M, $\lambda_{\text{ex}} = 380$ nm).

EPR experiments. Electron transfer reactions between POM-derivatives and MDEA are also evidenced by EPR spin-trapping (EPR-ST) experiments. EPR-ST is indeed the most valuable technique to observe radical species generated from photoinduced processes. In spin trapping experiments, the hyperfine splitting pattern and the values of the hyperfine coupling constants of the EPR spectrum of the spin adduct are characteristic of the type of free radical that is trapped.³¹ According to previous investigations,³² the irradiation of **POM-AB**/MDEA/DMPO (DMPO = 5,5-dimethyl-1-pyrroline N-oxide) solutions in acetonitrile under argon using a LED@400 nm source resulted in the generation of an EPR signal (Figure 7) representing the superposition of: i) a dominant signal characterized by the spin-Hamiltonian parameters ($a_N = 1.495 \pm 0.001$ mT, $a_{H\beta} = 1.745 \pm 0.01$ mT, $a_{H\gamma} = 0.136 \pm 0.01$ mT, $a_{H\delta} = 0.072 \pm 0.003$ mT; $g = 2.0057 \pm 0.0001$), assigned to the formation of a DMPO-adduct with carbon-centered radical on MDEA (called α -aminoalkyl radical) and ii) the second signal with the following

hyperfine coupling constants ($a_N = 1.486 \pm 0.004$ mT, $aH\beta = 2.127 \pm 0.01$ mT; $g = 2.0058 \pm 0.0001$) corresponds to a carbon-centered radical on phenyl group of the benzophenone moiety.³³ The intensity of both signals gradually increased upon the prolonged LED@400 nm irradiation.

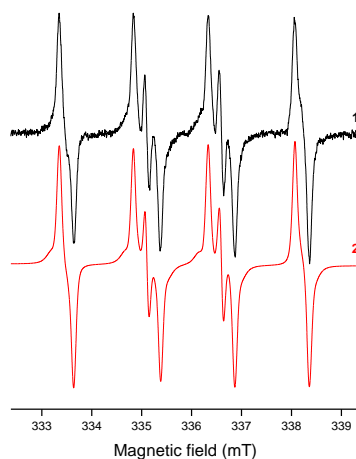


Figure 7. The normalized experimental (1) and simulated (2) EPR spectra obtained after 900 s LED@400 nm exposure of **POM-AB**/MDEA acetonitrile solutions in the presence of DMPO spin trapping agent under argon. The simulation best fit was calculated considering the relative concentration of $^{\bullet}$ DMPO-CR (aminoalkyl) and $^{\bullet}$ DMPO-carbon-centered radicals of 88 % and 12 %, respectively.

The generation of identical DMPO-adducts and gradual rise of their intensity was observed also upon LED@400 nm exposure of **POM-AC**/MDEA/DMPO (Figure S15) and **POM-AQ**/MDEA/DMPO (Figure S16) solutions in acetonitrile under argon. However, their stability in the experimental systems is low, and the prolonged/stopped irradiation led to a rapid decline, most probably due to the high reactivity of photoactivated system towards nitroxide moiety.

Photopolymerization studies with POM derivatives photoinitiating systems and polymer characterization

Free-radical photopolymerization. The use of polyoxometalates as photoinitiating systems has been scarcely studied.^{7-12,34} To date, most of the investigations have used two- or three-

component photo-initiating systems for free-radical polymerization of acrylates under UV light irradiation (Hg-Xe lamp), and to the best of our knowledge, no photoinitiating systems based on POMs have been designed for initiating radical photopolymerization under irradiation with wavelengths higher than 405 nm. This may be related to the fact that the POMs considered in the previous studies do not absorb significantly in the visible range. In the following experiments, we will demonstrate the capability of imido POM derivatives to promote free-radical photopolymerization (FRP) under visible LEDs irradiation. Table 2 summarizes the acrylate conversions of two functional acrylate monomers, namely TMPTA and SOA, with POM derivatives/MDEA photoinitiating systems under LEDs@385, 405, 455 or 470 nm irradiation. Kinetic profiles for the polymerization of acrylate monomers (TMPTA and SOA) under LED irradiation are displayed in Figures 8, S17, S18 and S19.

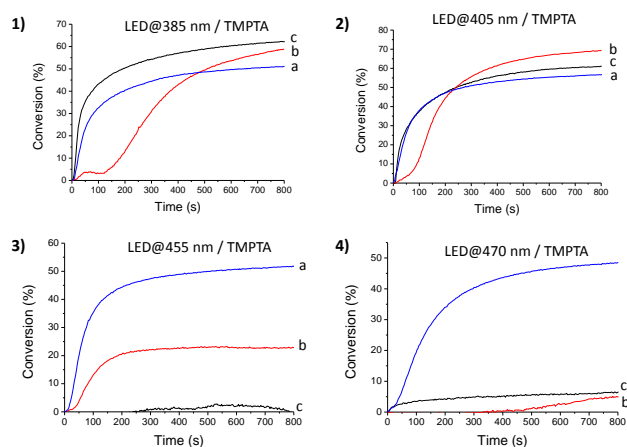


Figure 8. Kinetic profiles of TMPTA (acrylate group) in laminate in presence of **POM-AQ/MDEA** (a), **POM-AC/MDEA** (b) and **POM-AB/MDEA** (c) upon exposure with 1) LED@385 nm, 2) LED@405nm, 3) LED@455 nm and 4) LED@470 nm. Thickness of the film = 12 μm .

It evidences that the synthesized POM derivatives can show good initiating properties, likely due to the formation of aminoalkyl radical species as demonstrated by EPR ST technique (see above). Kinetics of polymerization are most effective in laminate than under air due to the oxygen inhibition of radicals

leading to a long period of inhibition. The **POM-AQ**/MDEA photo-initiating system appears as the most efficient likely due to the highly favorable electron transfer reaction (ΔG_S (POM-AQ/MDEA) = -1.1 eV) compared to that of **POM-AC** and **POM-AB** ones. Overall, it is observed that the photopolymerization process occurs under LED irradiation in the visible range, with wavelength ranging from 405 to 470 nm, which to our knowledge is a first example for the synthesis of such composites incorporating POMs.

Materials characterization. In this section, materials are synthesized with the best performing photo-initiating systems, i.e **POM-AQ**/MDEA. The synthesis of rectangular **POM-AQ** derived materials (**POM-AQ**/MDEA/SOA) are performed under LED@405 nm irradiation and under air, the obtained materials adopting a rectangular shape as a result of the fabrication method. DSC results demonstrate that no endothermic peak is observable, meaning that no further free-radical polymerization occurs during thermal analysis in the -80°C to 200°C range. It seems that free-radical photopolymerization of SOA is complete even under air. T_g is evaluated at around 14°C (Figure S20), which is similar to what is described in literature for UV-photoinduced SOA materials. Loading and unloading curves of the nanoindentation tests on **POM-AQ** coatings were overlapping, demonstrating an elastomeric behavior (Figure S21). Elastic modulus of **POM-AQ**-based coatings is measured by fitting the load/displacement curve by a pure elastic indentation model and was evaluated to 96 ± 18 MPa. Surprisingly, in the same conditions, the reference coatings based on the well-known UV photoinitiating system *i.e.* 2,2-Dimethoxy-2-phenylacetophenone (DMPA), did not lead to mechanically stable coatings for nanoindentation tests.

Table 2. TMPTA and SOA final acrylate conversions (%) obtained by RT-FTIR after 800 s of irradiation (LEDs@385, 405, 455 and 470 nm) under air and in laminate conditions, in the presence of PI/MDEA with PI = **POM-AC**, **POM-AB** or **POM-AQ**.

Photo-initiating system	LED@385 nm	LED@405 nm	LED@455 nm	LED@470 nm
Monomer: TMPTA				
POM-AC/MDEA	58% ^a , 55% ^{b*} (280s)	69% ^a , 68% ^b (130s)	23% ^a , 0% ^b	5% ^a
POM-AB/MDEA	62% ^a , 35% ^{b*} (360s)	60% ^a , 60% ^b (200s)	0% ^a , 0% ^b	6% ^a
POM-AQ/MDEA	51% ^a , 30% ^{b*} (30s)	57% ^a , 66% ^{b*} (50s)	52% ^a , 25% ^{b*} (200s)	50% ^a
Monomer: SOA				
POM-AC/MDEA	33% ^a , 0% ^b	69% ^a , 70% ^{b*} (34s)	26% ^a , 0% ^b	-
POM-AB/MDEA	9% ^a , 0% ^b	36% ^a , 0% ^b	18% ^a , 0% ^b	-

POM-AQ/MDEA	42% ^a , 8% ^b	90% ^a , 70% ^b	43% ^a , 15% ^b	25% ^a
-------------	------------------------------------	-------------------------------------	-------------------------------------	------------------

a = in laminate; b = under air; * (inhibition period in s under air)

Considering the scratch resistance tests, the height profiles before and after scratches appear similar, confirming thus the entire recovery of the **POM-AQ**-based coatings and its noteworthy elastomeric behavior (Figure S21). It can be proposed that addition of **POM-AQ** into the polymer matrix decreases the intermolecular forces into SOA films, thus improving their flexibility. Optical microscopy observation after scratches does not show any fracture, delamination, or residual imprint, demonstrating also a very good resistance to brittle fracture and adherence to the steel.

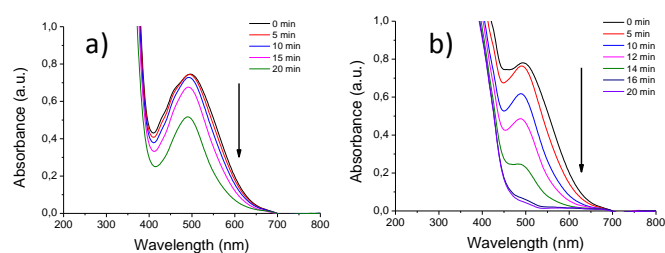


Figure 9. Photolysis experiments of a TPCPD solution a) in absence of **POM-AQ** and b) in the presence of **POM-AQ** during LED@405 nm exposure in acetonitrile. Light intensity = 25 mW/cm². [TPCPD] = 6.29 × 10⁻⁴ M and [POM-AQ] = 4.97 × 10⁻⁵ M.

Interestingly, the remarkable capacity of **POM-AQ** to generate singlet oxygen species in solution under LED@405 nm irradiation has been evidenced. The addition of **POM-AQ** in a tetraphenylcyclopentadienone (TPCPD) solution indeed leads to a tremendous decrease of the TPCPD absorbance in comparison with the **POM-AQ** solution-free reference (Figure 9), evidencing that the oxidation of TPCPD is due to the singlet oxygen species generated in presence of **POM-AQ**.³⁵ These interesting results prompted us to test **POM-AQ**-based coatings as antibacterial materials against *S. aureus* under solar light irradiation.

Prior to anti-bacterial tests, POM-derived surfaces were put into contact for 24h with a *S. aureus* solution to maximize bacterial adhesion. Interestingly, the incubated and irradiated surfaces show anti-adhesion property as the number of colony forming units (CFUs) for these surfaces are ten times lower than that observed with non-irradiated ones (Figure 10). Previous control experiments demonstrated that solar light has no influence on bacterial death.¹⁷ Interestingly, the antibacterial results also demonstrated that light has no significant influence on the proliferation of bacteria on the surface of related **POM-AQ** free materials as the CFUs for irradiated **POM-AQ** free materials is high, being similar to that observed for non-irradiated **POM-AQ** derived ones. As a consequence, singlet oxygen species produced under solar light activation at the surface of the POM-derived material is responsible for bacterial death. This interesting result undoubtedly demonstrates the potentialities of the POM-derived materials to be used for disinfection applications.

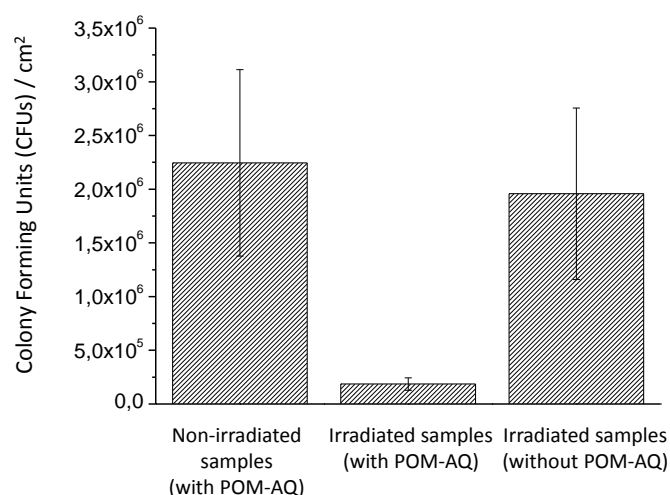


Figure 10. Colony forming units (CFUs) at the surface of the photoinduced derived material with and without **POM-AQ**, and after 2 h of solar light exposure (irradiated) and without light irradiation (non-irradiated).

CONCLUSION

In conclusion, we report herein a new synthetic strategy allowing shifting from UV to visible light the photoinitiating activity of organic aromatic molecules. Three imido-Lindqvist POMs obtained by reaction of amino derivatives of the anthracene, benzophenone and anthraquinone UV photosensitizers, respectively, and the $[\text{Mo}_6\text{O}_{19}]^{2-}$ POM precursor have been fully characterized in the

solid state and in solution. Notably, these compounds have been obtained in one step in a very short reaction time (1 h). Steady-state photolysis experiments evidenced a high interaction between the three reported hybrid POMs and MDEA, the reductive agent considered here for radical polymerization reactions. In addition, fluorescence studies highlight a favorable electron transfer process between the singlet excited state of **POM-AQ** and MDEA, while EPR investigations allow to characterize the MDEA-centered radical species generated from the photoinduced processes. Very importantly, the capability of such imido POM derivatives to promote free-radical photopolymerization even under visible LED irradiation was demonstrated. After 800s, acrylate conversion yields up to 50% under 470 nm LED irradiation for the **POM-AQ**/MDEA/TMPTA photoinitiating system and 90% under 405 nm LED irradiation for the **POM-AQ**/MDEA/SOA one were indeed observed, while in such conditions no polymerization was evidenced considering 2-aminoanthraquinone as photoinitiator. Rectangular films prepared considering the **POM-AQ**/MDEA/SOA photosystem have been obtained, the free-radical photopolymerization of SOA being complete even when performed in the presence of air. The coatings exhibit a very good flexibility, resistance to brittle fracture and adherence to stainless steel substrate. Also, **POM-AQ** exhibits a high capacity to generate singlet oxygen species in solution under visible light irradiation. Interestingly, investigation of the photoinduced antibacterial properties of the coatings against *S. aureus* put to the forefront its capability to limit bacterial adhesion. Overall, this work paves the way to the elaboration of a large range of easy-to-synthesize visible-light polymerization photoinitiators. Future work will focus on the preparation of related hybrids incorporating thiophene derivatives, which present very interesting photocatalytic and biological properties.³⁶ Also, while we report here on the synthesis of POM derivatives covalently bonded to one organic fragment, imido-Lindqvist POMs incorporating up to six organic fragments can be obtained.³⁷ Investigation of the effect of the accumulation of organic photoinitiators around a single Lindqvist unit on the properties of the hybrid systems thus seems very appealing.

ASSOCIATED CONTENT

Supporting Information. The Supporting Information is available free of charge at <https://pubs.acs.org/doi/xxx>. It includes details on the characterization methods, NMR, IR, ESI-MS, EPR ST and transition absorption spectra, crystallographic data, photolysis experiments, kinetic profiles for the free-radical photopolymerization of TMPTA and SOA, and nanoindentation tests experiments.

ACKNOWLEDGMENTS

This work was supported by the Ministère de l'Enseignement Supérieur et de la Recherche, the CNRS, the Université de Versailles Saint Quentin en Yvelines, the Université Paris-Est Créteil (UPEC) and the French National Research Agency (ANR PolyBact). We would like also to thank Prof. Vlasta Brezová for her help in ESR ST experiments. CampusFrance is gratefully acknowledged for its support through an Excellence Eiffel doctoral grant for ZH and by a mobility program PHC CEDRE (project POMBORON n°42237UG).

REFERENCES

- ¹ Miras, H. N.; Yan, J.; Long, D.-L.; Cronin, L. Engineering polyoxometalates with emergent properties. *Chem. Soc. Rev.* **2012**, *41*, 7403-7430.
- ² Proust, A.; Matt, B.; Villanneau, R.; Guillemot, G.; Gouzerh, P.; Izzet, G. Functionalization and post-functionalization: a step towards polyoxometalate-based materials. *Chem. Soc. Rev.* **2012**, *41*, 7605-7622.
- ³ Dolbecq, A.; Dumas, E.; Mayer, C.; Mialane, P. Hybrid Organic-Inorganic Polyoxometalate Compounds: From Structural Diversity to Applications. *Chem. Rev.* **2010**, *110*, 6009-6048.

- ⁴ Walsh, J. J.; Bond, A. M.; Forster, R. J.; Keyes, T. E. Hybrid polyoxometalate materials for photo(electro-) chemical applications. *Coord. Chem. Rev.* **2016**, *306*, 217-234.
- ⁵ Bijelic, A.; Aureliano, M.; Rompel, A. The antibacterial activity of polyoxometalates: structures, antibiotic effects and future perspective. *Chem. Commun.* **2018**, *54*, 1153-1169.
- ⁶ Wang, S.-S.; Yang, G.-Y. Recent advances in polyoxometalate-catalyzed reactions. *Chem. Rev.* **2015**, *115*, 4893-4962.
- ⁷ Lalevée, J.; Blanchard, N.; Tehfe, M.-A.; Fouassier, J.-P. Decatungstate ($W_{10}O_{32}^{4-}$)/Silane: A New and Promising Radical Source Under Soft Light Irradiation. *Macromol. Rapid Commun.* **2011**, *32*, 838–843.
- ⁸ Xiao, P.; Dumur, F.; Tehfe, M.-A.; Graff, B.; Fouassier J.-P.; Gigmes, D.; Lalevée, J. Keggin-Type Polyoxometalate ($[PMo_{12}O_{40}]^{3-}$) in Radical Initiating Systems: Application to Radical and Cationic Photopolymerization Reactions. *Macromol. Chem. Phys.* **2013**, *214*, 1749–1755.
- ⁹ Mokbel, H.; Simonnet-Jégat, C.; Dumur, F.; Gigmes, D.; Toufaily, J.; Hamieh, T.; Fouassier, J.-P.; Lalevée, J. Iodonium-polyoxometalate and thianthrenium-polyoxometalate as new one-component UV photoinitiators for radical and cationic polymerization. *J. Polym. Sci. Part A: Polym. Chem.* **2015**, *53*, 981-989.
- ¹⁰ Ghali, M.; Brahmi, C.; Benlifa, M.; Dumur, F.; Duval, S.; Simonnet-Jégat, C.; Morlet-Savary, F.; Jellali, S.; Bouselmi, L.; Lalevée, J. New hybrid polyoxometalate/polymer composites for photodegradation of eosin dye. *J. Polym. Sci. Part A: Polym. Chem.* **2019**, *57*, 1538-1549.
- ¹¹ Ghali, M.; Brahmi, C.; Benlifa, M.; Vulot, C.; Airoudj, A.; Fioux, P.; Dumur, F.; Simonnet-Jégat, C.; Morlet-Savary, F.; Jellali, S.; Bouselmi, L.; Lalevée, J. Characterization of polyoxometalate/polymer photo-composites: a toolbox for the photodegradation of organic pollutants. *J. Polym. Sci.* **2021**, *59*, 153-165.
- ¹² Brahmi, C.; Benlifa, M.; Ghali, M.; Dumur, F.; Simonnet-Jégat, C.; Monnier, V.; Morlet-Savary, F.; Bouselmi, L.; Lalevée, J. Performance improvement of the photocatalytic process for the degradation of pharmaceutical compounds using new POM/ polymer photocatalysts. *J. Environ. Chem. Eng.* **2021**, *9*, 106015.

- ¹³ Wei, Y.; Xu, B.; Barnes, C.; Peng, Z. An Efficient and Convenient Reaction Protocol to Organoimido Derivatives of Polyoxometalates. *J. Am. Chem. Soc.* **2001**, *123*, 4083–4084.
- ¹⁴ Zhu, Y.; Xiao, Z.; Ge, N.; Wang, N.; Wei, Y.; Wang, Y. Naphthyl Amines as Novel Organoimido Ligands for Design of POM-Based Organic–Inorganic Hybrids: Synthesis, Structural Characterization, and Supramolecular Assembly of (Bu₄N)₂[Mo₆O₁₈N(Naph-1)]. *Cryst. Growth Des.* **2006**, *6*, 1620–1625.
- ¹⁵ Hur, N. J.; Klemperer, W. G.; Wang, R. C. *Inorganic Synthesis*, Volume 27. Editor : Ginsberg, A. P. **1990**, 77. Copyright © 1990 Inorganic Syntheses, Inc.
- ¹⁶ Sautrot-Ba, P.; Brezová, V.; Malval, J.-P.; Chiappone, A.; Brelov, L.; Abbad Andaloussi, S.; Versace, D.-L. Purpurin derivatives as visible-light photosensitizers for 3D printing and valuable biological applications. *Polymer Chemistry* **2021**, *12*, 2627-2642.
- ¹⁷ Sautrot-Ba, P.; Jockussch, S.; Malval, J.-P.; Brezová, V.; Rivard, M.; Abbad-Andaloussi, S.; Blacha-Grzechnik, A.; Versace, D.-L. Quinizarin Derivatives as Photoinitiators for Free-Radical and Cationic Photopolymerizations in the Visible Spectral Range. *Macromolecules* **2020**, *53*, 1129–1141.
- ¹⁸ Sheldrick, G. M. SADABS, Program for Scaling and Correction of Area Detector Data, University of Göttingen, Germany, 1997.
- ¹⁹ Blessing, R. A., Empirical Correction for Absorption Anisotropy. *Acta Crystallogr.* **1995**, *A51*, 33-38.
- ²⁰ Sheldrick G. M. SHELX-TL, Software Package for the Crystal Structure Determination, Siemens Analytical X-ray Instrument Division, Madison, WI USA, 1994.
- ²¹ Breloy, L.; Brezová, V.; Richeter, S.; Clément, S.; Malval, J.-P.; Abbad Andaloussi, S.; Versace, D.-L. Bio-based porphyrins pyropheophorbide *a* and its Zn-complex as visible-light photosensitizers for free-radical photopolymerization. *Polymer Chemistry* **2022**, *13*, 1658-1671.
- ²² Stoll, S.; Schweiger, A. EasySpin, a comprehensive software package for spectral simulation and analysis in EPR. *J. Magn. Reson.* **2006**, *178*, 42–55.
- ²³ Mendes Marinho, S.; Ha-Thi, M.-H.; Pham, V.-T.; Quaranta, A.; Pino, T.; Lefumeux, C.; Chamailé, T.; Leibl, W.; Aukauloo, A. Time-Resolved Interception of Multiple-Charge Accumulation in a Sensitizer–Acceptor Dyad. *Angew. Chem. Int. Ed.* **2017**, *56*, 15936-15940.

- ²⁴ Mazeran, P.-E.; Beyaoui, M.; Bigerelle, M.; Guigon, M. Determination of mechanical properties by nanoindentation in the case of viscous materials. *Int. J. Mater. Res.* **2012**, *103*, 715-722.
- ²⁵ Haider, T.; Shyshov, O.; Suraeva, O.; Lieberwirth, I.; von Delius, M.; Wurm, F. R. Long-Chain Polyorthoesters as Degradable Polyethylene Mimics. *Macromolecules* **2019**, *52*, 2411–2420.
- ²⁶ Al-Yasari, A.; Van Steerteghem, N.; El Moll, H.; Clays, K.; Fielden, J. Donor–acceptor organo-imido polyoxometalates: high transparency, high activity redox-active NLO chromophores. *Dalton Trans.* **2016**, *45*, 2818-2822.
- ²⁷ Al-Yasari, A.; Van Steerteghem, N.; Kearns, H.; El Moll, H.; Faulds, K.; Wright, J. A.; Brunchwitz, B. S.; Clays, K.; Fielden, J. Organoimido-Polyoxometalate Nonlinear Optical Chromophores: A Structural, Spectroscopic, and Computational Study. *Inorg. Chem.* **2017**, *56*, 10181–10194.
- ²⁸ Al-Yasari, A.; Spence, P.; El Moll, H.; Van Steerteghem, N.; Horton, P. N.; Brunchwitz, B. S.; Clays, K.; Fielden, J. Fine-tuning polyoxometalate non-linear optical chromophores: a molecular electronic "Goldilocks" effect. *Dalton Trans.* **2018**, *47*, 10415-10419.
- ²⁹ Al-Yasari, A.; El Moll, H.; Purdy, R.; Vincent, K.B.; Spence, P.; Malval, J.P.; Fielden, J. Optical, third order non-linear optical and electrochemical properties of dipolar, centrosymmetric and C_{2v} organoimido polyoxometalate derivatives. *Phys. Chem. Chem. Phys.* **2021**, *23*, 11807-11817.
- ³⁰ Dahiya, P.; Kumbhakar, M.; Maity, D. K.; Mukherjee, T.; Mittal, J. P.; Tripathi, A. B. R.; Chattopadhyaya N.; Pal, H. Photophysical properties of 2-amino-9,10-anthraquinone: evidence for structural changes in the molecule with solvent polarity. *Photochem. Photobiol. Sci.* **2005**, *4*, 100-105.
- ³¹ Peyrot, F.; Lajnef, S.; Versace, D.-L. Electron Paramagnetic Resonance Spin Trapping (EPR–ST) Technique in Photopolymerization Processes. *Catalysts* **2022**, *12*, 772.
- ³² Boulmier, A.; Haouas, M.; Tomane, S.; Michely, L.; Dolbecq, A.; Vallée, A.; Brezová, V.; Versace, D.-L.; Mialane, P.; Oms, O. Photoactive Polyoxometalate/DASA Covalent Hybrids for Photopolymerization in the Visible Range. *Chem. Eur. J.* **2019**, *25*, 14349 – 14357.
- ³³ Barker, P.; Bechwith, A. L. J.; Cherry, W. R.; Huie, R. Characterization of spin adducts obtained with hydrophobic nitron spin traps. *J. Chem. Soc., Perkin Trans. 2*, 1985, 1147-1150

- ³⁴ Xiao, P.; Simmonet-Jégat, C.; Dumur, F.; Schrodj, G.; Tehfe, M.-A.; Fouassier J.-P.; Gigmes, D.; Lalevée, J. Photochemical *in situ* elaboration of polyoxometalate (α -[SiMo₁₂O₄₀]⁴⁻)/polymer hybrid materials. *Polym. Chem.* **2013**, *4*, 4526-4530.
- ³⁵ P. H. Marek-Urban, M. Urban, M. Wiklinska, K. Paplinska, K. Woźniak, A. Blacha-Grzechnik, K. Durka. Heavy-Atom Free spiro Organoboron Complexes As Triplet Excited States Photosensitizers for Singlet Oxygen Activation. *J. Org. Chem.* **2021**, *86*, 12714-12722.
- ³⁶ Vallan, L.; Istif, E.; Jéniffer Gómez, I.; Alegret, N.; Mantione, D. Thiophene-Based Trimers and Their Bioapplications : An Overview. *Polymers* **2021**, *13*, 1977.
- ³⁷ Huang, Y.; Zhang, J.; Hao, J.; Wei, Y. A general and highly regioselective synthesis approach to multifunctionalized organoimido derivatives of Polyoxometalates. *Sci. Rep.* **2016**, *6*, 24759.